Supplementary Information

Insights into $Ti_3N_2T_2/VS_2$ (T = F, O, OH) heterostructures as innovative anode materials for lithium/sodium/magnesium-ion batteries

Feng-Ming Ma,[a] Xiao-Meng Zhao,[a] Han-Bai Luo,[a] Chun-Liang Shang,[a] Hui-Min Gao,[b] Xiao-Lin Wang*[a]

[a] Key Laboratory of Cluster Science of the Ministry of Education, Beijing Key Laboratory of Photoelectronic/Electrophotonic Conversion Materials, School of Chemistry and Chemical Engineering, Beijing Institute of Technology, Beijing 102488, China

[b] State Key Laboratory of Supramolecular Structure and Materials, Institute of Theoretical Chemistry, Jilin University, Changchun, 130023, China

* Email: wangxl614@bit.edu.cn

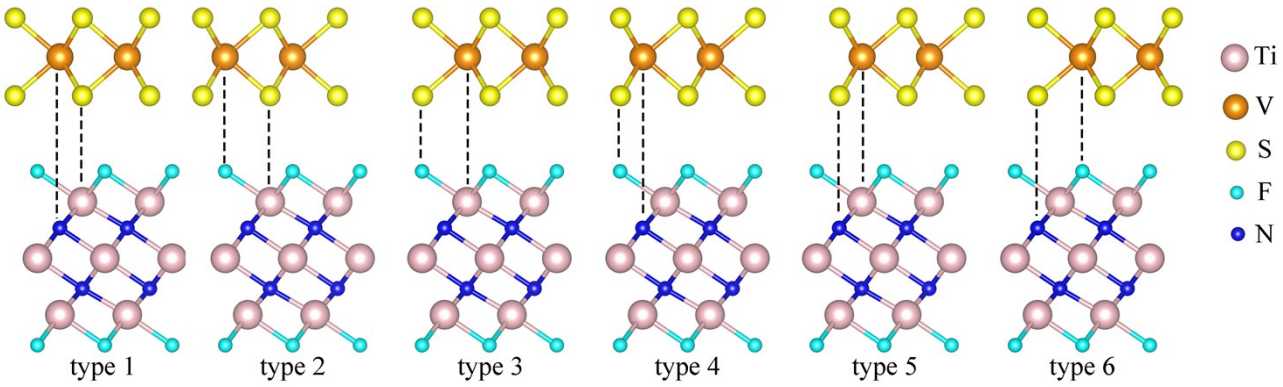

Fig. S1 Side views of the initial $Ti_3N_2F_2/VS_2$ heterostructures with six stacking patterns.

Table S1 Binding energies E_b (eV) and interlayer distances d (Å) of the optimized $Ti_3N_2T_2/VS_2$ (T = F, O, OH) heterostructures with different stacking patterns.

Heterostructure	Pattern	E_b	d
$Ti_3N_2F_2/VS_2$	type 1	−0.75	2.68
	type 2	−0.74	2.69
	type 3	−0.49	3.11
	type 4	−0.49	3.11
	type 5	−0.72	2.70
	type 6	−0.71	2.75
$Ti_3N_2O_2/VS_2$	type 1	−0.69	2.71
	type 2	−0.71	2.72
	type 3	−0.45	3.09
	type 4	−0.44	3.12
	type 5	−0.69	2.73
	type 6	−0.67	2.78
$Ti_3N_2(OH)_2/VS_2$	type 1	−3.14	1.78
	type 2	−3.17	1.74
	type 3	−3.45	1.93
	type 4	−3.46	1.92
	type 5	−3.10	1.79
	type 6	−3.14	1.76

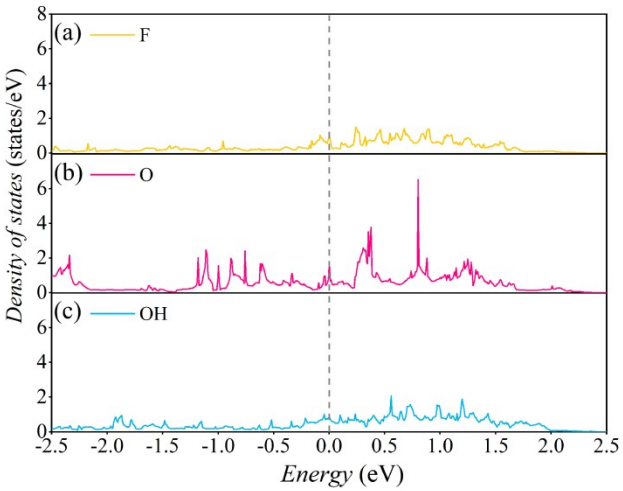

Fig. S2 Density of states of (a) F termination of $Ti_3N_2F_2/VS_2$, (b) O termination of $Ti_3N_2O_2/VS_2$ and (c) OH termination of $Ti_3N_2(OH)_2/VS_2$, where the Fermi levels are set to zero.

Table S2 Adsorption energies E_{ad} (eV) and change rates of interlayer distances $\triangle d/d$ (%) of individual ions absorbed on the optimal $Ti_3N_2T_2/VS_2$ (T = F, O, OH) heterostructures.

Heterostructure	Site	Li		Na		Mg	
		E_{ad}	$\triangle d/d$	E_{ad}	$\triangle d/d$	E_{ad}	$\triangle d/d$
$Ti_3N_2F_2/VS_2$	T1	−0.72	0.13	−0.84	−0.69	0.43	−0.51
	T2	−1.74	1.50	−1.46	0.42	−0.57	1.25
	T3	−1.59	1.49	−1.43	0.38	−0.44	1.22
	M1	−1.50	26.46	−1.31	50.66	−0.78	28.71
	M2	−1.88	19.02	−1.59	48.06	−1.34	28.61
	M3	−2.07	8.43	−1.84	35.33	−1.82	11.43
	B1	−0.43	0.02	−0.24	−0.51	1.56	−0.61
	B2	0.33	−0.24	0.11	−0.76	1.37	−0.53
	B3	−0.35	−0.65	−0.24	0.32	1.55	−0.76
$Ti_3N_2O_2/VS_2$	T1	−0.76	−0.14	−0.88	−0.93	0.43	−0.68
	T2	−1.75	−0.01	−1.48	−1.13	−0.53	−0.28
	T3	−1.59	1.00	−1.45	0.08	−0.40	0.85
	M1	−2.08	27.22	−1.96	53.78	−2.35	29.83
	M2	−2.39	22.34	−2.01	55.43	−2.46	30.06
	M3	−2.53	9.49	−2.31	37.36	−3.14	13.87
	B1	−1.86	0.06	−1.64	−0.34	−0.85	−0.16
	B2	−0.95	0.32	−0.83	0.00	0.58	−0.04
	B3	−1.62	−0.03	−1.49	−0.37	−0.44	−0.23
$Ti_3N_2(OH)_2/VS_2$	T1	−0.66	−0.44	−0.82	−0.77	0.42	0.35
	T2	−1.72	−0.19	−1.42	−0.89	−0.59	−0.18
	T3	−1.55	−0.11	−1.39	−0.80	−0.44	0.06
	M1	−0.82	2.62	−0.16	11.47	0.23	6.14
	M2	a	a	a	a	a	a
	M3	−1.06	1.63	−0.38	9.61	−0.15	4.34
	B1	0.21	0.21	0.38	0.13	1.53	−0.15
	B2	0.72	−0.02	0.14	−0.12	1.15	−0.03
	B3	0.47	−0.13	0.42	−0.31	1.04	0.01

[a] A metal ion was initially located at the M2 site, but was adsorbed at the M3 site after optimization.

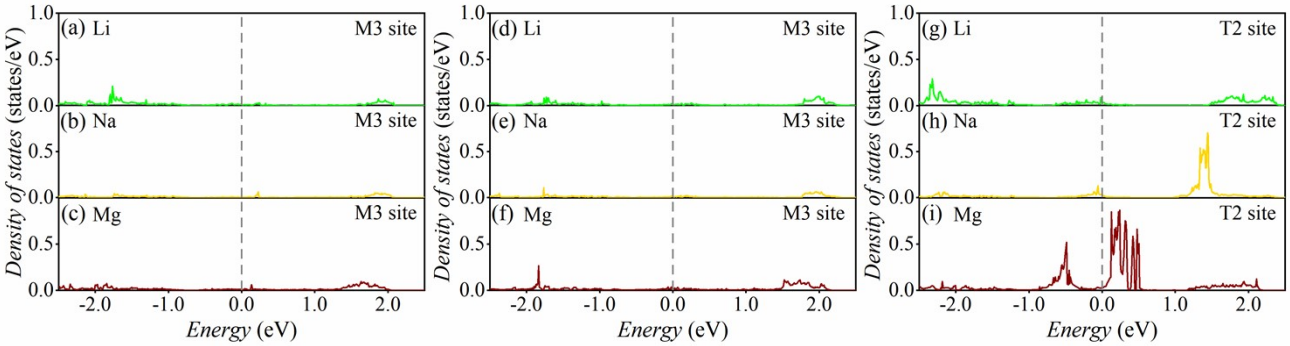

Fig. S3 Total density of states of each adsorbed ion derived from (a)−(c) $Ti_3N_2F_2/VS_2$ adsorption systems, (d)−(f) $Ti_3N_2O_2/VS_2$ adsorption systems and (g)−(i) $Ti_3N_2(OH)_2/VS_2$ adsorption systems. All the Fermi levels are shifted to zero for comparison.

Table S3 The Fermi levels (eV) of the most stable pristine and single ion-adsorbed $Ti_3N_2T_2/VS_2$ (T = F, O, OH) heterostructures.

Heterostructure	No ion	Li	Na	Mg
$Ti_3N_2F_2/VS_2$	−0.73	−0.66	−0.59	−0.47
$Ti_3N_2O_2/VS_2$	−1.11	−1.00	−0.92	−0.87
$Ti_3N_2(OH)_2/VS_2$	0.19	0.87	1.23	1.10

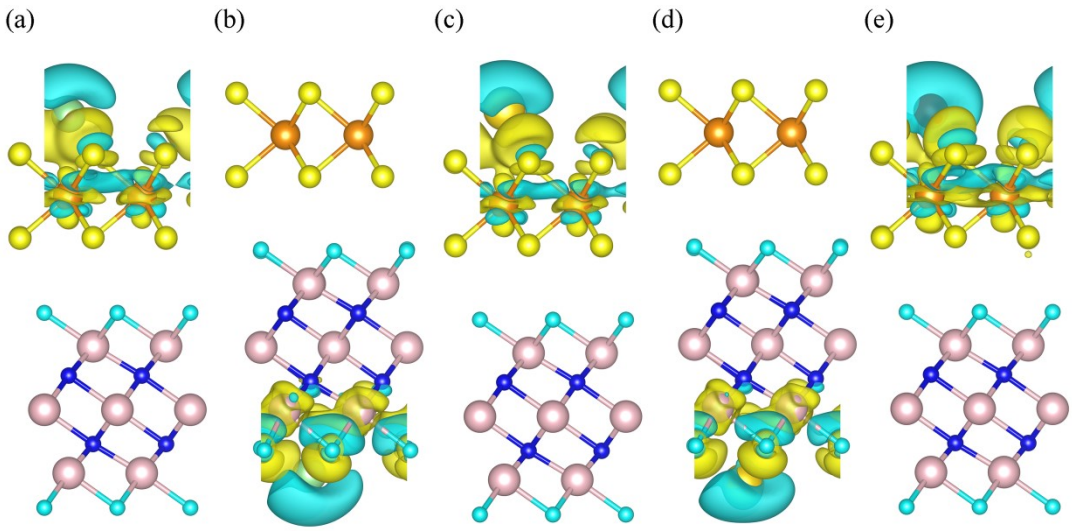

Fig. S4 Charge density difference of individual Li/Na/Mg ions adsorbed at the most favorable sites of the upper and lower surfaces of $Ti_3N_2F_2/VS_2$. (a) Li^+, (c) Na^+ and (e) Mg^{2+} bound to the T2 site, and (b) Li^+, (d) Na^+ bound to the B1 site, respectively. The yellow and cyan represent charge accumulation and depletion, respectively. The isosurface value is set to 0.008 *e* $Å^{-3}$.

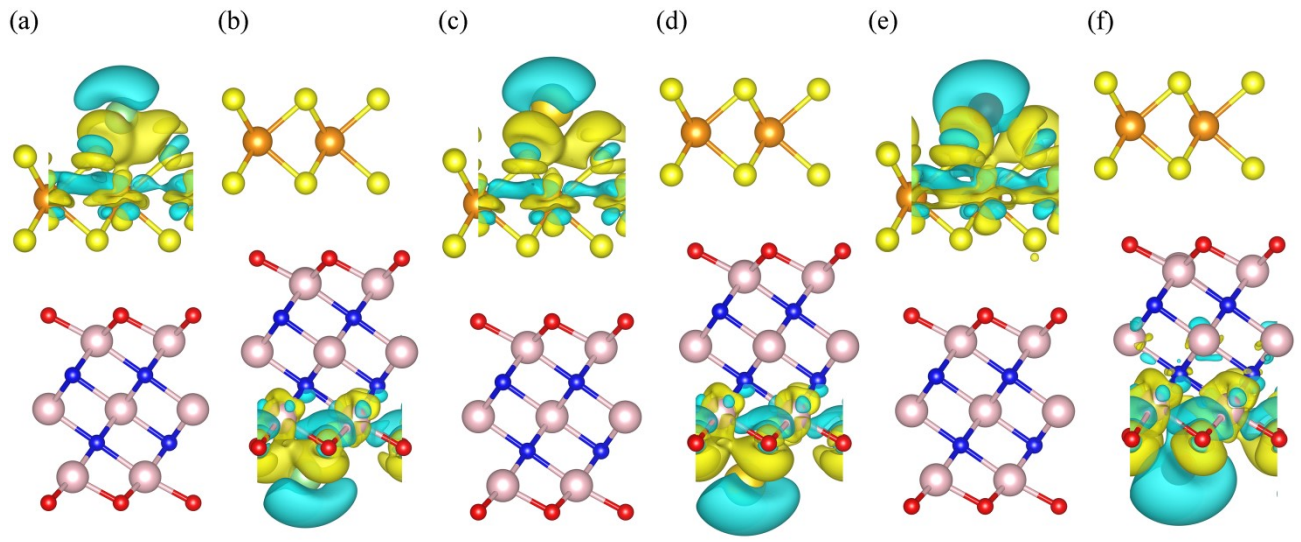

Fig. S5 Charge density difference of individual Li/Na/Mg ions adsorbed at the most favorable sites of the upper and lower surfaces of $Ti_3N_2O_2/VS_2$. (a) Li^+, (c) Na^+ and (e) Mg^{2+} bound to the T2 site, and (b) Li^+, (d) Na^+ and (f) Mg^{2+} bound to the B1 site, respectively. The yellow and cyan represent charge accumulation and depletion, respectively. The isosurface value is set to 0.008 *e* $Å^{-3}$.

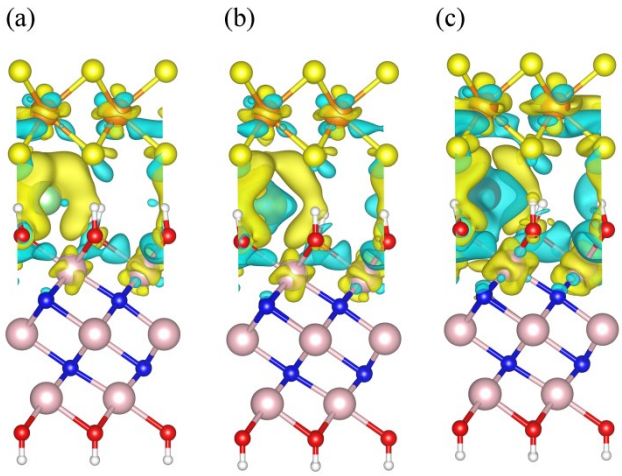

Fig. S6 Charge density difference of (a) Li^+, (b) Na^+ and (c) Mg^{2+} adsorbed at the most favorable M3 site of the interlayer of $Ti_3N_2(OH)_2/VS_2$, respectively. The yellow and cyan represent charge accumulation and depletion, respectively. The isosurface value is set to 0.008 *e* $Å^{-3}$.

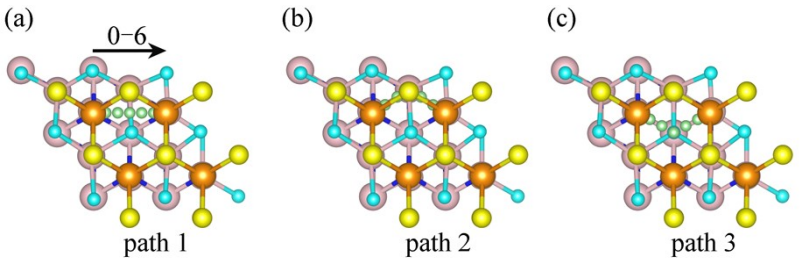

Fig. S7 Top views of three diffusion paths of a metal ion (green ball) between two adjacent M3 sites of $Ti_3N_2F_2/VS_2$. Each path contains seven images marked as 0−6 from left to right.

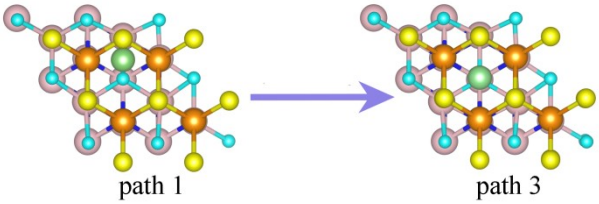

Fig. S8 Ion position (green ball) in the fourth image changes after optimization, causing the diffusion path of each ion at the interface of $Ti_3N_2F_2/VS_2$ to transform from linear path to fold-line path.

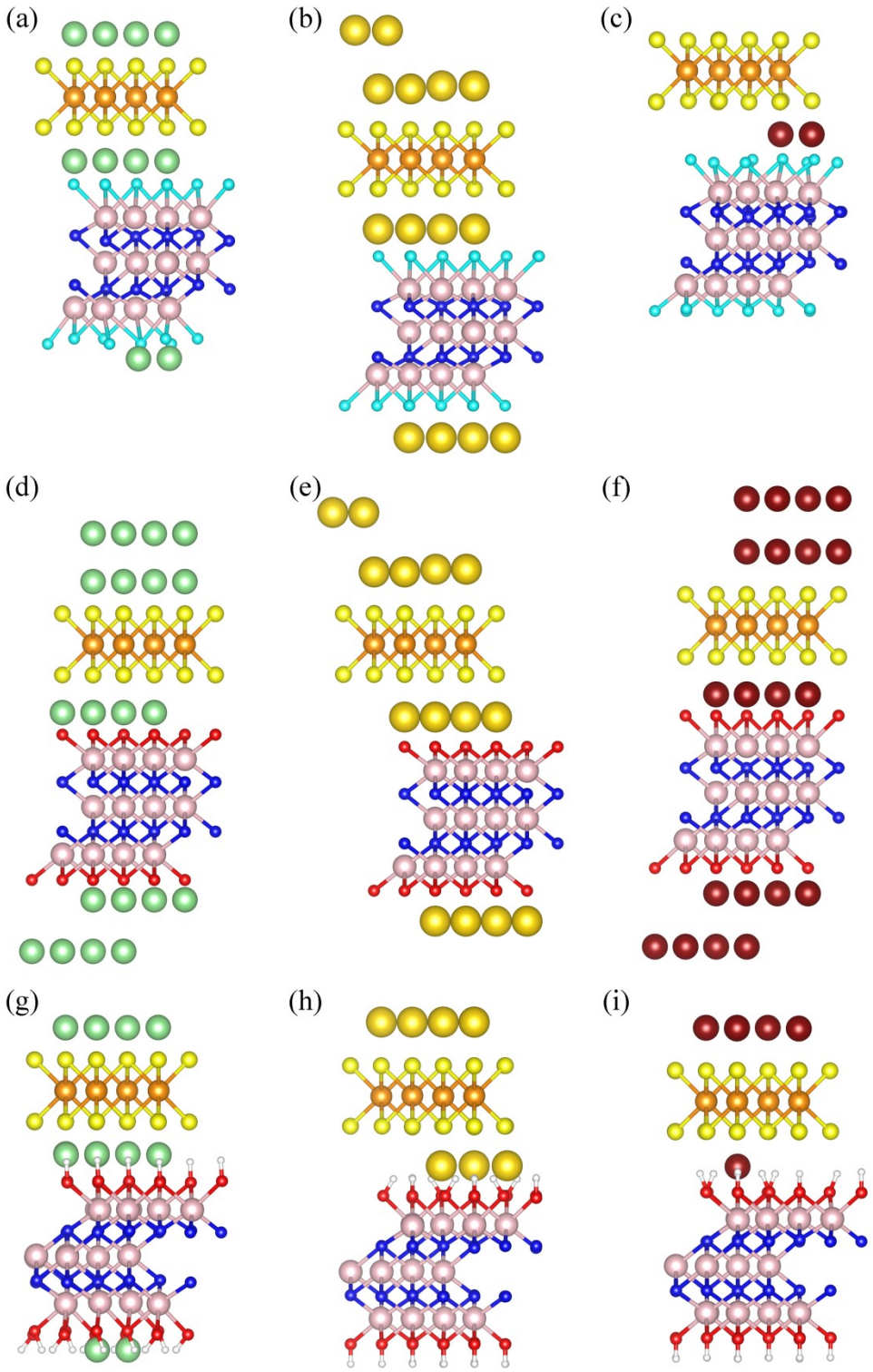

Fig. S9 Structures corresponding to the maximum load concentrations of Li/Na/Mg ions adsorbed on $Ti_3N_2T_2/VS_2$ (T = F, O, OH). Side views of (a) $Ti_3N_2F_2/VS_2Li_{2.5}$, (b) $Ti_3N_2F_2/VS_2Na_{3.5}$, (c) $Ti_3N_2F_2/VS_2Mg_{0.5}$, (d) $Ti_3N_2O_2/VS_2Li_5$, (e) $Ti_3N_2O_2/VS_2Na_{3.5}$, (f) $Ti_3N_2O_2/VS_2Mg_5$, (g) $Ti_3N_2(OH)_2/VS_2Li_{2.5}$, (h) $Ti_3N_2(OH)_2/VS_2Na_{1.75}$, (i) $Ti_3N_2(OH)_2/VS_2Mg_{1.25}$.

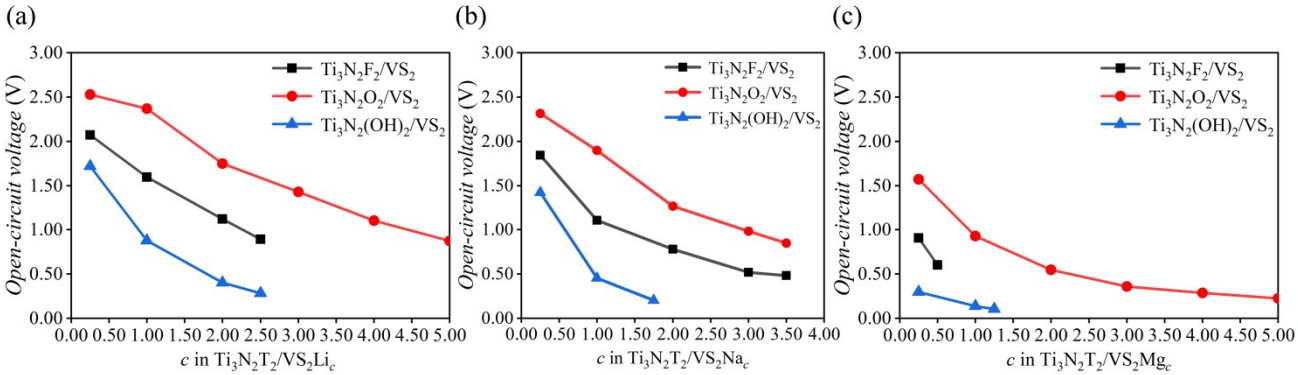

Fig. S10 OCV as a function of the stoichiometric ratio (c) of ion concentration in $Ti_3N_2T_2/VS_2A_c$ for (a) LIBs, (b) SIBs, and (c) MIBs, respectively.